Solar driven photocatalysis using iron and chromium doped TiO2 coupled to moving bed biofilm process for olive mill wastewater treatment

Solar driven photocatalysis using iron and chromium doped TiO_2 coupled to moving bed biofilm process for olive mill wastewater treatment

Antonietta Mancuso[1], Nicola Morante [1], Marco De Carluccio[2], Olga Sacco[3], Luigi Rizzo[2*], Vincenzo Vaiano[1*], Diana Sannino[1]

[1] Department of Industrial Engineering, University of Salerno, Via Giovanni Paolo II 132, 84084 Fisciano (SA), Italy

[2] Water Science and Technology group (WaSTe), Department of Civil Engineering, University of Salerno, Via Giovanni Paolo II 132, 84084 Fisciano (SA), Italy

[3] Department of Chemistry and Biology "A. Zambelli", University of Salerno, Via Giovanni Paolo II, 132, 84084 Fisciano (SA), Italy

*Corresponding authors: Vincenzo Vaiano, vvaiano@unisa.it; Luigi Rizzo, l.rizzo@unisa.it

Abstract

TiO_2 based-photocatalysts doped with Fe and/or Cr was evaluated as pre- and post-treatment method of a moving bed biofilm reactor (MBBR) as possible solution for the treatment of real olive oil mill wastewater (OMW). Photocatalysts were synthesized by sol-gel method and their chemical-physical properties were accurately investigated through X-ray diffraction (XRD), Raman spectroscopy, UV–Vis diffuse reflectance spectroscopy (UV–Vis DRS) and specific surface area measurements. UV–Vis DRS measurements evidenced that the simultaneous doping of TiO_2 lattice with Fe and Cr improves the optical absorption into the visible region leading to a narrow band gap (2.1 eV) with respect to undoped TiO_2 (3.2 eV) and Fe-doped TiO_2 (2.8 eV) while, Cr-doped TiO_2 showed the lowest bandgap value (1.9 eV). XRD patterns and Raman spectra showed that anatase is the

predominant crystalline phase for all the prepared photocatalysts and Fe and Cr ions were effectively inserted into the TiO_2 lattice. The TiO_2 doping with Cr did not change the average crystallites size that was equivalent to that of TiO_2 (8 nm), whereas, for Fe- doped TiO_2, it was lower than the others and equal to 6 nm. The specific surface area values of doped catalysts were higher than TiO_2 and the value for Fe-Cr-codoped TiO_2 resulted to be 97 $m^2 g^{-1}$. Photocatalytic treatment of OMW was evaluated in terms of total polyphenols (TPHs), Chemical Oxygen Demand (COD), Biological Oxygen Demand (BOD_5) and biodegradability (as BOD_5/COD ratio) in 3 h of treatment under simulated solar light irradiation. Fe-doped TiO_2 showed the highest TPHs removal ~~efficiency~~ for both un-treated and biologically treated OMW. When H_2O_2 was added (optimum dosage 0.5g L^{-1}), Fe-Cr-TiO_2 resulted in the best photocatalytic performance with TPHs removal ~~efficiency~~ as high as 97% and increased biodegradability (0.22 to 0.33), making the effluent suitable for the subsequent biological process. When photocatalytic process was investigated as post-treatment of OMW, Fe-TiO_2 showed the best activity and the addition of 0.5 g L^{-1} of H_2O_2 was sufficient to make the effluent in compliance with Italian regulation for effluent disposal into surface water.

Keywords

doped TiO_2; moving bed biofilm reactor; olive mill wastewater treatment; polyphenols; solar photocatalysis; wastewater biodegradability.

1 Introduction

The world production of olive oil is about 3 million tons per year, and it is represented by more than 87% in the Mediterranean basin and about 69% in Europe, in particular in Spain, Greece, and Italy, as estimated by “International Olive Council”. Accordingly, one of the major issues of such agro-industrial activity is the production of olive mill wastewater (OMW) which is estimated between 7-30 million m^3 per year [1-3] and it is really challenging to treat with conventional processes [1]. The composition of OMW can vary greatly and depends on the type of olives processed, their maturity,

and the type of process used for oil extraction (pressing or centrifugation) [4]. ~~Generally, OMW treatment is challenging for two main reasons. First of all, the high pollutant load (in terms of chemical oxygen demand (COD)) together with a high concentration of recalcitrant compounds (lignin and tannins), long-chain fatty acids, and phenolic compounds make it difficult to treat OMW~~ Generally, OMW treatment is challenging for two main reasons: the high chemical oxygen demand (COD) together with a high concentration of recalcitrant compounds (lignin and tannins), long-chain fatty acids, and phenolic compounds [5] and the seasonality ~~Secondly, the production of olive oil is seasonal and this means that a large amount of OMW is produced in a very short time~~ [6]. Furthermore, the phenolic compounds contribute to toxicity and inhibit bacterial activity in wastewater. This complicates the use of biological processes that usually require stable conditions and long acclimatization times. In particular, aerobic and anaerobic biological processes can only be used when the wastewater COD is not very high, such as in the case of olive-washing wastewater [7]. Among biological processes, activated sludge is the most used one, but requires a separation of the sludge from the treated wastewater and sludge recirculation to keep the process under proper biomass concentration. Additionally, the efficiency of this process can be impaired by the bulking phenomenon, an obstacle to sludge settling/separation, which can be attributed to large amounts of lipid substrates, low contents of dissolved oxygen, and acidic pH (typical features for OMW) [8]. Another biological process investigated in the OMW treatment is membrane technology. However, it is also characterized by some limitations compared to other biological processes, including: (i) fouling formation of the membrane, (ii) short membrane lifetimes and (iii) high costs [9]. Unlike of biological suspended growth processes, biofilm based technologies do not require sludge recirculation. Among them, moving bed biofilm reactors (MBBRs) have been investigated for the treatment of acidic and phenolic wastewater, showing good phenols removal and great stability against hydraulic and toxic shock loads [10-12]. The growing concern for OMW toxic effects and the drawbacks of the available processes and technologies has increased the interest among scientists to

find effective treatment solutions to ensure their safe disposal into the environment [13]. In order to successfully treat such challenging wastewater a proper strategy is to couple chemical and biological processes. Among chemical processes, advanced oxidation processes (AOPs) are known for their ability to effectively remove refractory pollutants thanks to the generation of reactive oxygen species (ROS) at room temperature and ambient pressure [14]. In particular, the phenolic compounds were found to be degradable by UV light driven photocatalysis and photo Fenton [15-19]. To save energy, even more desirable in this period due to the continuous increase in its cost, solar driven photocatalysis appears to be an attractive option among AOPs [20]. Titanium dioxide (TiO_2) is possibly the most investigated semiconductor in heterogeneous photocatalytic applications to water and wastewater treatment. TiO_2 is non-toxic, highly active and stable under a wide range of chemical conditions, making it an ideal photocatalyst for these applications [21-25]. However, TiO_2 is activated only in the presence of UV light irradiation. Due to its wide band gap energy (3.2 eV), it could not be effectively activated by sunlight which contains 2 – 3% of UV light, 40 – 43 % of visible light, and 50 – 55 % of infrared light [26]. In addition, the low surface area and poor adsorption capacity of TiO_2 as well as the high rate of recombination of photogenerated electron-hole pairs on semiconductor surface, limit its photocatalytic activity [27]. A possible strategy to solve such limitations as well as to increase the efficiency of the photocatalytic activity is the doping of TiO_2 lattice with metal elements [28-32].

In this work different TiO_2-based photocatalysts (co)doped with metal elements (Fe and Cr) (namely TiO_2, Fe-TiO_2, Cr-TiO_2, and Fe-Cr-TiO_2) activated by sunlight were investigated in combination to MBBR as pre- and post-treatment method of real OMW. The photocatalysts were synthesized by sol-gel method and their chemical-physical properties were investigated through X-ray diffraction (XRD), Raman spectroscopy, UV–Vis diffuse reflectance spectroscopy (UV–Vis DRS) and specific surface area measurements. The effect of solar photocatalysis as pre-treatment method was evaluated in terms of total polyphenols (TPHs), Chemical Oxygen Demand (COD) and Biological Oxygen

Demand (BOD_5) removals and effect on OMW biodegradability (as BOD_5/COD ratio). The effect of photocatalytic process as post-treatment method was investigated in terms of TPHs removal, this being the main challenge to make the effluent in compliance with the corresponding limit for disposal into the environment. Photocatalytic tests in presence of hydrogen peroxide, varying the oxidant dosage to maximize the degradation of phenolic compounds as well as wastewater biodegradability were also carried out. OMW was mixed to synthetic urban wastewater before MBBR treatment to simulate a co-treatment scenario in a multi-barrier approach. It is worth noting that, despite the availability of some papers about the photocatalytic treatment of OMW using N-doped TiO_2 [33-35], Ni doped C/TiO_2 [36] and ZrO_2-doped TiO_2 nanocomposite [37], to authors' knowledge, no study is available in the scientific literature about real OMW treatment by photocatalysis based on TiO_2 co-doped with metal elements under sunlight. Furthermore, there are no works in the literature concerning the combination of MBBR and photocatalysis for the treatment of real OMW.

2 Materials and methods

2.1 Chemicals and reagents

Titanium tetraisopropoxide ($C_{12}H_{28}O_4Ti$ > 97% (w/w)), Sigma Aldrich), chromium (III) nitrate nonahydrate ($Cr(NO_3)_3 \cdot 9H_2O \geq 99\%$), iron acetylacetonate ($[CH_3COCH=C(O)CH_3]_2Fe \geq 99.95\%$, Sigma Aldrich), sodium carbonate anhydrous ($Na_2CO_3 \geq 99\%$, Riedel-de Haën), hydrogen peroxide solution (H_2O_2, 30% (w/w) in H_2O, Sigma Aldrich), titanium(IV) oxysulfate solution ($TiOSO_4$ ~ 15% (w/w) in dilute sulfuric acid ≥ 99.99%, Sigma Aldrich), hydrochloric acid solution (HCl, 37% (w/w) in H_2O, Carlo Erba) and distilled water (Carlo Erba) were purchased and used as received. The reagents for the preparation of synthetic wastewater, Ferric chloride hexahydrate ($FeCl_3 \cdot 6H_2O$) 97%, Magnesium sulphate heptahydrate ($MgSO_4 \cdot 7H_2O$), Glucose, Sucrose, Ammonium sulphate ($(NH_4)_2SO_4$), Ammonium chloride (NH_4Cl), Potassium dihydrogen phosphate (KH_2PO_4), Potassium hydrogen phosphate (K_2HPO_4), Manganese sulphate hydrate ($MnSO_4 \cdot H_2O$), Sodium bicarbonate ($NaHCO_3$), Calcium chloride hexahydrate ($CaCl_2 \cdot 6H_2O$) were purchased from Carlo Erba.

2.2 Preparation of photocatalysts

TiO_2, Fe-doped TiO_2, Cr-doped TiO_2, and Fe-Cr co-doped TiO_2 photocatalysts were synthesized through the sol-gel method using iron(II) acetylacetonate as precursor for iron, chromium(III) nitrate nonahydrate as precursor for chromium, and titanium tetraisopropoxide (TTIP) as precursor for TiO_2. Undoped TiO_2 was prepared using distilled water and a solution containing titanium tetraisopropoxide, whereas Fe-doped TiO_2 (Fe-TiO_2) photocatalyst was obtained by reaction between distilled water and a solution containing titanium tetraisopropoxide and iron acetylacetonate. Chromium-doped TiO_2 (Cr-TiO_2) photocatalyst was synthetized through sol-gel method using an aqueous solution of chromium(III) nitrate nonahydrate and adding the TTIP dropwise into the solution.

To prepare Fe-Cr co-doped TiO_2 (Fe-Cr-TiO_2) catalysts, distilled water containing a certain amount of chromium(III) nitrate nonahydrate were mixed with a solution of titanium tetraisopropoxide and iron(II) acetylacetonate. The system was maintained at room temperature under continuous stirring for 10 min. The obtained suspension was centrifuged for the separation of the precipitate, which was washed with distilled water three times and finally placed in a furnace at 450 °C for 30 min in static air. The Fe/Ti and Cr/Ti molar ratio used for the preparation of Fe-TiO_2 and Cr-TiO_2 was equal to 0.0017 and 0.0188, respectively, and correspond to an optimized catalyst formulation as reported in previous works [38, 39]. The Fe-Cr-TiO_2 photocatalyst was made using the optimal precursor loads of iron (25 mg) and chromium (318 mg). Table S1 (see Supplementary Material) reports the solution volume, the amount of Fe and Cr precursors used for the synthesis together with the weight percentage of iron and chromium for each prepared catalyst.

2.3 Chemical-physical characterization of photocatalysts

The ultraviolet-visible diffuse reflectance spectra (UV-Vis DRS) of the catalysts were recorded using a Perkin Elmer spectrometer Lambda 35 spectrophotometer with a RSA-PE-20 reflectance spectroscopy accessory (Labsphere Inc., North Sutton, NH). The band gap values of the catalysts

were calculated through the corresponding Kubelka–Munk function (KM) and by plotting (KM × $h\nu^2$) against hν. The average crystallite size of the synthesized powders was determined using Scherrer's equation [40]. The Brunauer Emmett and Teller (BET) surface area of the catalysts was measured through dynamic N_2 adsorption measurement at -196 °C, by a Costech Sorptometer 1042 after pre-treatment for 30 min in He flow at 150 °C. X-ray diffraction (XRD) patterns were performed with an automatic Bruker D8 Advance diffractometer (VANTEC-1 detector) using reflection geometry and nickel filtered Cu-Kα radiation. Laser Raman spectra were obtained at room temperature with a Dispersive MicroRaman (Invia, Renishaw), equipped with 514 nm laser, in the range 100 - 2000 cm^{-1} Raman shift.

2.4 OMW sample

The OMW sample was taken in an oil mill located in the province of Salerno (southern Italy). The oil mill used a 3-phase oil extraction system. The characteristics of the sample are summarized in Table 1. Given the high solids content, the sample was centrifuged for 30 min at 5000 rpm before the experiments. The centrifuged sample was diluted (1/70) with deionized water before the photocatalysis experiments when it was investigated as pre-treatment to MBBR. When photocatalysis was investigated as post-treatment method, the same centrifuged sample was diluted 1/100 with synthetic urban wastewater (SWW) before treatment with MBBR to simulate OMW co-treatment in an urban WWTP (Figure S1 in Supplementary Material). The SWW was prepared according to a well-known protocol [41].

Table 1 OMW sample characteristics.

Parameters	Raw Sample	After centrifugation
pH	4.7	4.7
COD (g L^{-1})	126.9	87.1

TSS (g L^{-1})	21	3
TPHs (g L^{-1})	7.1	5
BOD_5 (g L^{-1})	29.2	20
BOD_5/COD	0.24	0.23

2.5 MBBR

The MBBR consisted in a cylindrical reactor with an internal diameter of 9 cm. The water height in the reactor was 40 cm with a total volume of 2.5 L. The reactor was filled through bio-carriers with the following characteristics: size of 10.5 (Φ) ×8 mm (h), density of 0.15 g cm^{-3}, specific surface area of 9500 m^2 m^{-3} and protected surface of 500 m^2 m^{-3}. The filling ratio of bio-carriers was around 35% as this turned out to be the maximum value to allow fluid movement of the bio-carriers inside the reactor. An air pump was used to provide dissolved oxygen for the biological process and turbulence to keep the bio-carriers suspended in the reactor. The air was introduced through a stone diffuser positioned at the bottom of the reactor. The system was operated in batch mode, the reactor being filled and emptied daily.

A bacterial inoculum, taken from a real activated sludge process in a WWTP located in Salerno, was used for the start-up phase of the biofilm growth. The sludge was obtained from the recirculation line of the aeration tank and was acclimated for 1 day with the SWW before the inoculation. The initial biomass concentration in the bioreactor was around 3.0 g L^{-1}. After the inoculation the MBBR was fed with the SWW in batch mode for 2 months, until biofilm formation was observed. Once the biofilm growth started, the reactor was no longer inoculated and fed with SWW until the COD removal ~~efficiency~~ stabilized. Finally, the MBBR was fed with the solution of OMW diluted 1/100 with SWW. During the experiment, pH and dissolved oxygen were monitored. The biomass concentration in the reactor was evaluated according to a previously published protocol [42]. BOD_5, COD, and TPHs were monitored in the effluent of the MBBR after 24 h of treatment. ~~and the corresponding removal efficiencies were calculated according to Eq.1:~~

~~$Z\ removal\ efficiency\ (t) = \left(1 - \frac{Z(t)}{Z_0}\right) * 100$ Eq.1~~

~~Where Z(t) is the parameter value after 24 h of HRT and Z_0 is the initial parameter value in the solution.~~

2.6 Photocatalytic activity tests

The photocatalytic activity of Cr-TiO_2, Fe-TiO_2 and Fe-Cr-TiO_2 catalysts was tested under simulated solar irradiation. The photocatalytic tests were conducted in a cylindrical photoreactor (ID = 2.6 cm, L_{TOT} = 41 cm, and V_{TOT} = 200 mL) equipped with: (i) an air distributor device (flow rate of 150 Ncm^3 min^{-1}), (ii) four solar lamps (SUN-GLO, nominal power 8 W each) placed equidistant (30 mm) from the external surface of the photoreactor to irradiate uniformly the volume of the solution; (iii) a peristaltic pump (Watson Marlow) to maintain the suspension continuously recirculated and to avoid the sedimentation of photocatalytic powder at the bottom of the reaction system (Figure S2 in Supplementary Material).

In a typical photocatalytic test, the treated solution volume was 100 mL at spontaneous pH and the photocatalyst dosage was 3 g L^{-1}. This dosage was optimized in our previous work by using the same photoreactor configuration [43]. Before the irradiation, the suspension was left in dark for 60 min to reach the adsorption/desorption equilibrium of the pollutants on the photocatalyst surface, and subsequently, the lamps were turned on to start photocatalytic test under simulated solar irradiation for 180 min. Photocatalytic process was investigated (i) as possible pre-treatment step before biological process on diluted OMW and (ii) as post-treatment (polishing step) after biological process (MBBR treatment of OMW mixed to SWW (TOMW)). Finally, the photocatalysts with the higher treatment performances were also investigated in presence of different dosages of H_2O_2 (Table 2) added just after the dark phase. At the end of each experimental test, the withdrawn OMW solution (or TOMW solution) was centrifuged at 5000 rpm for 3 min to remove the photocatalyst.

Table 2. Set-up of the experimental tests with OMW and TOMW solutions.

Experiment	Solution type	Photocatalyst	H_2O_2 dosage [g L^{-1}]
E1	OMW	TiO_2	0
E2	OMW	Fe-TiO_2	0
E3	OMW	Cr-TiO_2	0
E4	OMW	Fe-Cr-TiO_2	0
E5	OMW	Fe-TiO_2	0.75
E6	OMW	Fe-Cr-TiO_2	0.75
E7	OMW	Fe-Cr-TiO_2	0.5
E8	OMW	Fe-Cr-TiO_2	0.25
E9	TOMW	TiO_2	0
E10	TOMW	Fe-TiO_2	0
E11	TOMW	Cr-TiO_2	0
E12	TOMW	Fe-Cr-TiO_2	0
E13	TOMW	Fe-TiO_2	0.75
E14	TOMW	Fe-TiO_2	0.5
E15	TOMW	Fe-TiO_2	0.25

The samples before and after photocatalytic treatment were analyzed in terms of pH, TPHs, COD, BOD_5 and residual hydrogen peroxide.

The potential leaching of the metals from the doped photocatalysts during the catalytic tests was assessed by analysing the solution by ICP-AES (Varian Liberty II).

2.7 Analytical measurements

pH was measured using pH-meter PC 62 DHS (XS Instruments). The residual H_2O_2 was removed after treatment to prevent interference in the measurement of BOD_5 and COD, through the addition of an aqueous solution of concentrated sodium carbonate (300 g L^{-1}), according to the method proposed by Wu et al. [44]. Total phenols were analysed on filtered samples using the spectrophotometric method associated with the Folin-Ciocalteu phenol reagent [45]. Specifically, 10 mL of wastewater sample was mixed with 0.5 mL of Folin-Ciocalteu reagent and 1.5 mL of a sodium carbonate solution (200 g L^{-1}). The final solution was kept in dark for 60 min (20 °C) and

afterward, the absorbance of the solution was measured at 750 nm (Perkin Elmer spectrometer Lambda 25).

COD was analyzed according to the CNR-IRSA method 5135, using a HACH LCK cuvette.

BOD_5 was measured according to the CNR-IRSA method 5120 using an OXITOP® system.

3 Results and discussion

3.1 Photocatalysts characterization

The optical properties of the catalysts are reported in Figure 1. In detail, Figure 1a shows the UV-Vis diffuse reflectance spectra of TiO_2, Cr-TiO_2, Fe-TiO_2 and Fe-Cr-TiO_2 photocatalysts in terms of Kubelka-Munk function vs wavelength. While undoped TiO_2 was found to absorb mainly in the UV region, Cr-TiO_2 and Fe-TiO_2 and Fe-Cr-TiO_2 absorbed in the visible light region. The extended absorption in the visible region for the photocatalysts doped with Fe or Cr ions may be due to the charge-transfer transition between the d-electrons of dopant elements and the conduction band of TiO_2 according to their respective energy levels [46]. However, the absorption spectra of the modified TiO_2 in the visible region may also result from the presence of defects related to the oxygen vacancies that give rise to coloured centres [47-50]. Moreover, additional absorption bands in the range 600-800 nm can be observed for Cr-TiO_2 and Fe-Cr-TiO_2. Such absorption can be attributed to the $^4A_{2g} \rightarrow {}^4T_{2g}$ d–d transition of Cr^{3+} in the TiO_2 structure [51]. This result could correspond to the distance between the doping levels of the Cr^{3+} ions and the conduction band [51].

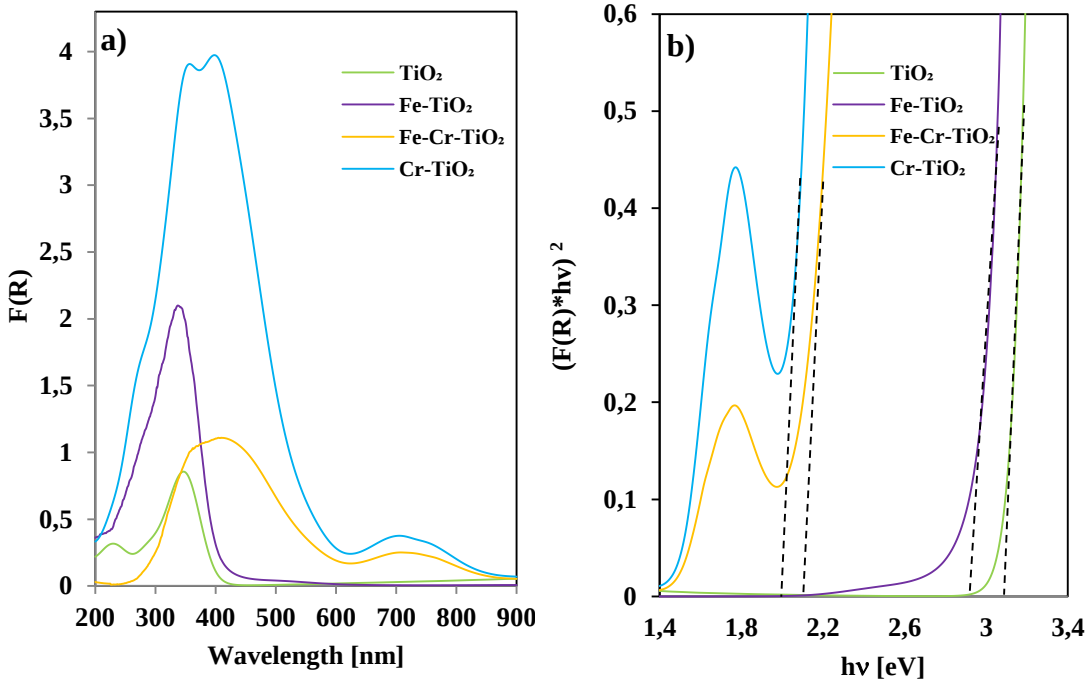

Figure 1. Reflectance spectra vs wavelength (a) and band gap calculation by UV–VIS DRS spectra (b) for TiO_2, Cr-TiO_2, Fe-TiO_2 and Fe-Cr-TiO_2 photocatalysts.

The band gap (E_{bg}) values for all prepared catalysts were calculated from UV-Vis measurements using the Kubelka-Munk function (~~Figure 2~~b). A large band gap (3.2 eV) for undoped TiO_2 and an E_{bg} value for the Fe-TiO_2 catalyst of about 2.8 eV was observed, while a remarkable decrease of E_{bg} value up to 1.9 eV with Cr-TiO_2 photocatalyst was obtained (Table 3). As expected, an E_{bg} value (2.1 eV) higher than Cr-TiO_2 but lower than Fe-TiO_2, was observed for Fe-Cr codoped TiO_2 photocatalyst. This result can be explained by the presence of Cr and Fe into the TiO_2 lattice which allows to extend the absorption of electromagnetic radiation in the visible range [52, 53].

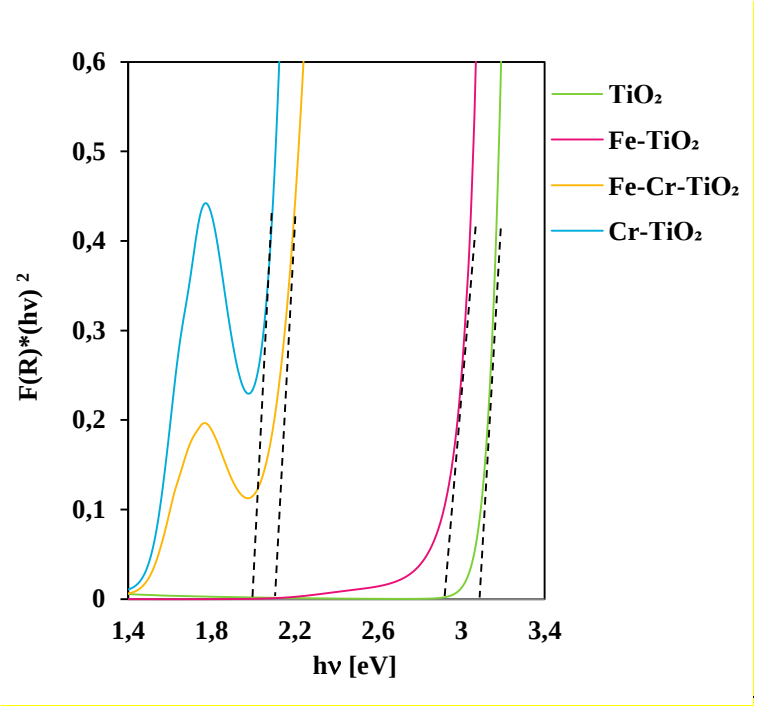

~~**Figure 2. Band gap calculation by UV–VIS DRS spectra for TiO_2, Cr-TiO_2, Fe-TiO_2 and Fe-Cr-TiO_2 photocatalysts.**~~

XRD spectra for TiO_2, Fe-TiO_2, Cr-TiO_2 and Fe-Cr-TiO_2 photocatalyst are plotted in Figure 2. In detail, undoped TiO_2 presents the typical peaks of the anatase phase with the main signal located at $2\theta = 25.91°$ (Figure a) [54].

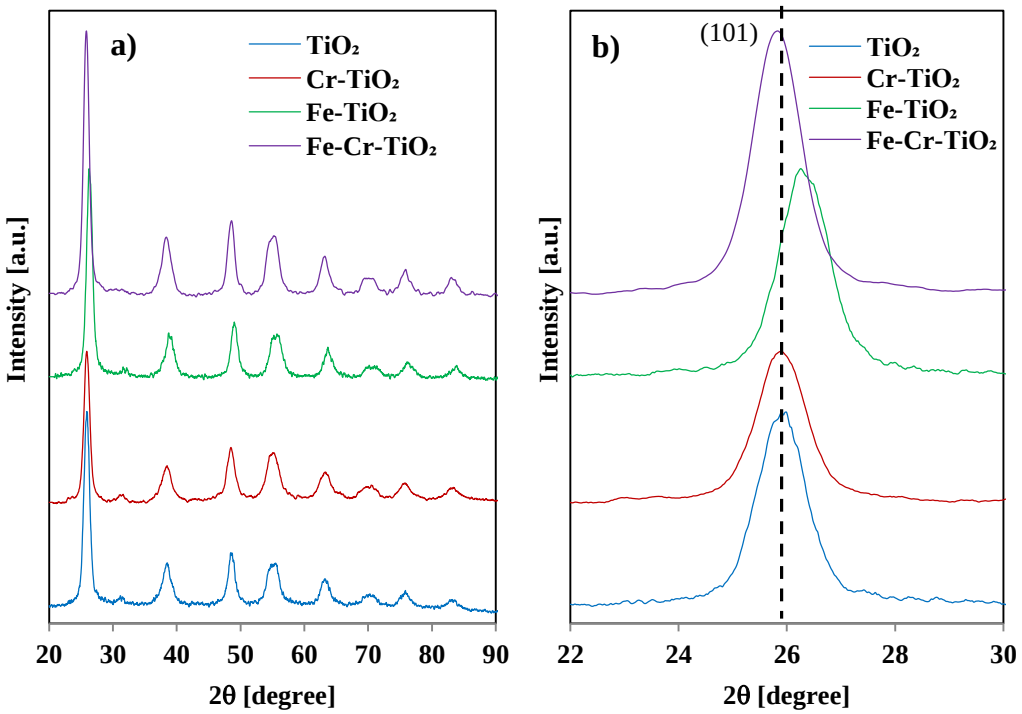

Figure 2. XRD patterns for TiO_2, Cr-TiO_2, Fe-TiO_2 and Fe-Cr-TiO_2 photocatalysts in the range 2θ = 20–80° (a) and in the range 2θ = 22–30° (b).

The XRD patterns of Fe-TiO_2, Cr-TiO_2 and Fe-Cr-TiO_2 also showed the characteristic peaks associated with the anatase crystalline phase of undoped TiO_2. No peaks of rutile phase were observed because the transformation from anatase to rutile phase did not take place. However, a typical signal associated to brookite phase was observed at about 2θ = 31° [55] in the XRD patterns of all synthesized photocatalysts. Furthermore, the diffraction patterns of the Fe-TiO_2, Cr-TiO_2 and Fe-Cr-TiO_2 did not show the presence of iron oxides [56], chromium titanates (such as Cr_2TiO_5 or $CrTiO_3$) [57] and chromium oxide (Cr_2O_3) [58], confirming the possible presence of Cr and Fe cations into TiO_2 lattice. In the case of Cr based photocatalysts, Ti^{4+} ion can be successfully substituted by Cr^{3+} since Ti^{4+} ion has a similar ionic radius (0.68 Å) of Cr^{3+} ion (0.69 Å) favouring Cr ions incorporation into the lattice without significant change in crystallite size [59]. Indeed, Cr-TiO_2 photocatalyst presents the equivalent crystallite size of undoped TiO_2 corresponding to 8 nm (Table 3). However, Ti^{4+} ions in the TiO_2 structure were replaced with Fe^{3+} because the ionic radius of Fe^{3+} (0.64 Å) is

smaller than the ionic radius of Ti^{4+} (0.68 Å) [60], leading to the ~~This phenomenon leads to a~~ decrease of crystallite size [61] and ~~Noteworthy,~~ to the shift in the peak corresponding to anatase (1 0 1) plane ~~for Fe-TiO_2~~ from 2θ = 25.91° to 2θ = 26.11° for Fe-TiO_2 catalyst ~~was observed~~ (Figure b). Noteworthy, the typical anatase signal for Cr-doped TiO_2 did not show a notable shift with respect to the undoped TiO_2, probably due to the similar ionic radius of Ti and Cr ions. Similar to Cr-TiO_2, Fe-Cr codoped TiO_2 did not show an appreciable shift of the peak associated with anatase phase compared to that of undoped TiO_2. The specific surface area (S_{BET}) of all catalysts measured by the BET method is provided in the Table 3. The value of the S_{BET} for Fe doped photocatalyst is higher than that of the undoped TiO_2 because of the smaller crystallite size of Fe-TiO_2. On the other hand, the S_{BET} of Cr-TiO_2 is quite similar to undoped TiO_2 whereas Fe-Cr co-doped TiO_2 is lower than the corresponding values observed for Fe-TiO_2, Cr-TiO_2 and undoped TiO_2, probably because of the possible presence of Cr_2O_3 on TiO_2 surface, as evidenced by Raman analysis (Figure 3).

Table 3. Crystallite size, specific surface area (S_{BET}) and band gap (E_{bg}) of all prepared photocatalysts.

Catalyst	Crystallite size [nm]	E_{bg} [eV]	S_{BET} [m^2g^{-1}]
TiO_2	8	3.2	107
Cr-TiO_2	8	1.9	113
Fe-TiO_2	6	2.8	122
Fe-Cr-TiO_2	8	2.1	97

Raman spectra in the range of 100–900 cm^{-1} for undoped TiO_2, Cr-doped TiO_2, Fe-TiO_2 and Fe-Cr-TiO_2 photocatalysts are reported in Figure . Raman bands were observed at 144, 397, 516 and 638 cm^{-1} together with a weak shoulder at 195 cm^{-1} in the spectra of all photocatalysts, indicating that anatase was the main crystalline structure [61]. The individual metal oxide bands were absent not only in the Fe-TiO_2 spectrum but also in Cr-doped TiO_2 and Fe-Cr-codoped TiO_2 spectra [62, 63].

Chromium oxide could exist in various forms such as CrO_3, Cr_8O_{21}, Cr_5O_{12}, CrO_2, Cr_2O_3, Cr_3O_4, CrO, and Cr_3O, due to the different oxidation states of the element. Bands at 648 cm^{-1}, 607 cm^{-1}, 548

cm^{-1}, 348 cm^{-1}, and 303 cm^{-1} are the Raman modes of Cr_2O_3, among these the stronger signal is 548 cm^{-1}; whereas, the broad peaks at 691 cm^{-1} and 856 cm^{-1} can be attributed to amorphous CrO_2 and either CrO_3 or Cr_8O_{21}, respectively [62]. The absence of bands at 691 cm^{-1} and 856 cm^{-1} indicates the absence of chromium oxides in high valence state. Meanwhile the very weak signals at 303 and 550 cm^{-1} in the spectra of Cr-TiO_2 and Fe-Cr-TiO_2, especially for the first one, could be attributed to a very low presence of Cr_2O_3, which however remains near to the detection limit.

This result is in agreement with the XRD results, suggesting that the metals (Cr and/or Fe) replaced or occupied positions in the TiO_2 framework rather than being present as impurities on the external surface of photocatalysts [49, 64, 65].

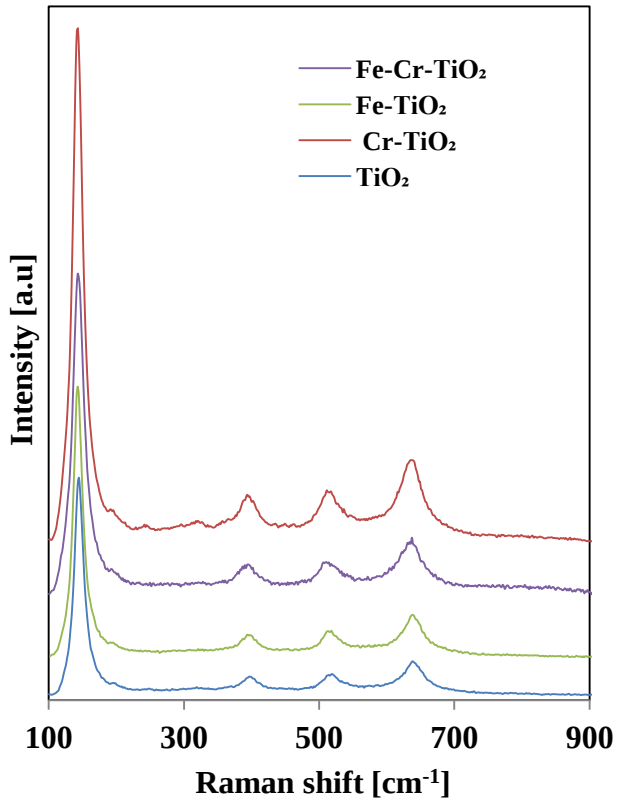

Figure 3. Raman spectra of TiO_2, Cr-TiO_2, Fe-TiO_2 and Fe-Cr-TiO_2 photocatalysts.

3.2 OMW treatment by MBBR and photocatalysis

3.2.1 OMW treatment by MBBR

The MBBR was fed by SWW for 15 days after stable removal efficiencies were observed. The concentrations of COD and BOD_5 of the SWW were 555.5 ± 2.5 mg L^{-1} and 300 ± 20 mg L^{-1}. After this phase, the MBBR was fed by OMW diluted (1%) with SWW for 40 days. Stabilization of MBBR performances required 11 days. During this phase the biomass concentration increased from 14 g L^{-1} to 25.9 g L^{-1}. The concentrations of TPHs, COD, BOD_5 in the OMW diluted with SWW were 42.8 ± 8.2 mg L^{-1}, 1221.1 ± 63.2 mg L^{-1} and 765 ± 56.3 mg L^{-1}, respectively.

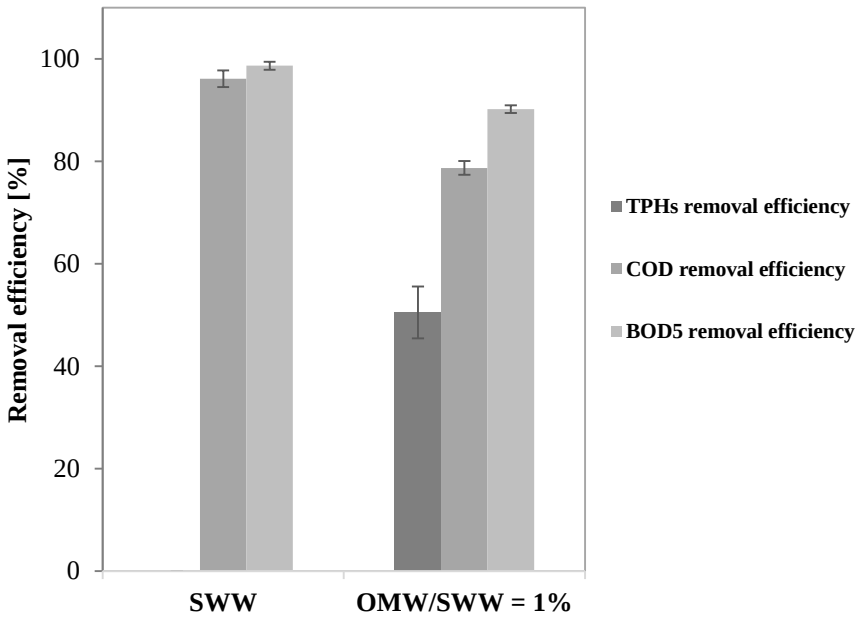

Figure 4 TPHs, COD and BOD_5 removal ~~efficiencies~~ [%] after 24h treatment of SWW and OMW/SWW with MBBR.

The COD and BOD_5 removal ~~efficiency~~ in the SWW phase were 96.1 ± 1.7% and 98.7 ± 0.8% respectively (Figure). This result is in agreement with a previous work on the formation of biofilm in MBBR for the treatment of urban wastewater [66]. In this work, the COD removal ~~efficiency~~ was 94% in 24 h of treatment with a filling ratio of 30%. The MBBR, after the first 11 days of acclimatization to the OMW solution, showed a removal ~~efficiency~~ of COD and BOD_5 equal to 78.7 ± 1.3% and 90.2 ± 1.0% respectively (Figure). The COD removal was higher than that observed in

a previous study on the treatment of palm oil mill effluent (similar to OMW in terms of characterization) by MBBR. Indeed, after 24 h with a filling ratio of 50% the removal ~~efficiency~~ was 54% [67]. The fairly high performances can be explained by the increased biodegradability (BOD_5/COD=0.63) due to the dilution with SWW. The TPHs removal was 50.5 ± 5.1%, but according to a previous work on the treatment of synthetic wastewater with high concentration of phenol (800 mg/l), better removal could be possible with sufficiently long acclimatization times for a switching of the bacterial community on phenol-degrading bacteria [11]. The performances of the MBBR process are not sufficient to meet the Italian regulatory limits (annex 5, third part, D.Lgs n. 152 /2006) for effluent disposal into surface water (Phenol = 0.5 mg L^{-1}; COD = 160 mg L^{-1}; BOD_5 = 40 mg L^{-1}). Therefore, photocatalysis treatment was also investigated as polishing step after MBBR treatment. The characteristics of TOMW are summarized in Table 4. Two treatment options were investigated for photocatalytic process: (i) as pre-treatment step on untreated diluted OMW and (ii) as polishing step on diluted OMW mixed to SWW and treated by MBBR (TOMW). Table 4 provides the characterization of diluted OMW and TOMW solutions used as the initial sample for the investigation of photocatalytic process as pre-treatment and polishing step, respectively.

Table 4. Characterization of diluted OMW and TOMW solutions used as the initial sample for photocatalytic tests.

Solutions	pH	TPHs [mg/L]	BOD_5 [mg_{O2}/L]	COD [mg_{O2}/L]	BOD_5/COD
OMW	5.5	100	370	1680	0.22
TOMW	7.5	14	80	275	0.29

3.2.2 OMW pre-treatment by photocatalysis

Higher removal ~~efficiency~~ of THPs, COD, and BOD_5 was observed for Fe-TiO_2 and Fe-Cr-TiO_2 compared to Cr-TiO_2 in OMW treatment (Figure 5). However, all these photocatalysts did not significantly affect biodegradability of OMW sample. In particular, such photocatalysts showed a TPHs removal ~~efficiency~~ of 39% and 32%, respectively, and a value of BOD_5/COD ratio after 3 h of irradiation equal to 0.23 for both samples. Higher performance of Fe-TiO_2 and Fe-Cr-TiO_2 photocatalysts under solar light irradiation is supported by the decrease of band gap, 2.8 eV and 2.1 eV, respectively, measured by UV-Vis analysis (Figure 1). The poor efficiency of solar-driven Cr-TiO_2 treatment, the photocatalyst being characterized by the lowest band gap value (1.9 eV), could be explained by a significant recombination rate of photogenerated hole-electron pairs [27]. The other factor that could negatively affect the photocatalytic efficiency of Cr-TiO_2 is that the slight lower S_{BET} of this photocatalyst results in a lower amount of active sites on the catalyst surface. Furthermore, the presence of traces of Cr_2O_3 phase on the surface of the doped photocatalyst could be unfavourable to the adsorption and, as a consequence, to the photocatalytic degradation of organic pollutants. ~~On the other hand, despite undoped TiO_2 sample showed interesting removal efficiency with regard to the target parameters, it resulted in a faster degradation of BOD_5 compared to COD, further reducing OMW biodegradability (0.22 to 0.20) and making undoped TiO_2 not appropriate for the pre-treatment of OMW.~~

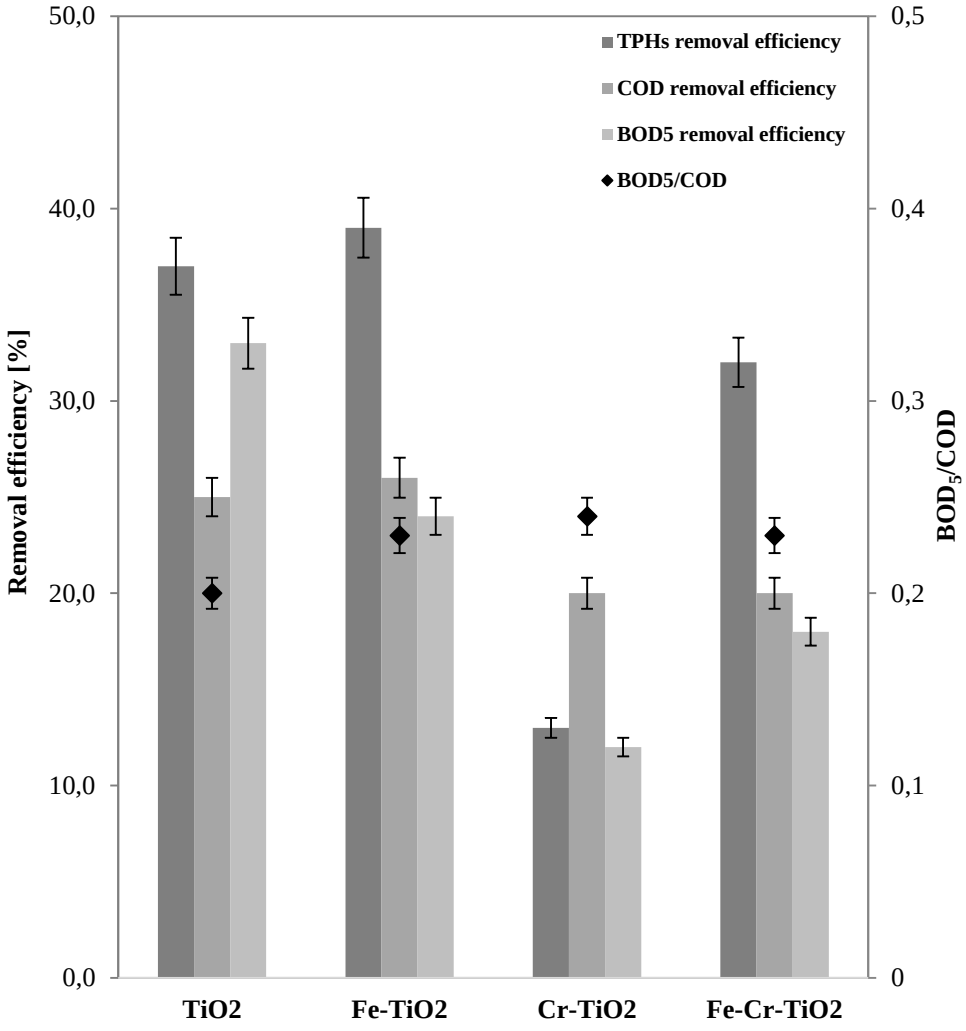

Figure 5. TPHs, COD, BOD_5 removal ~~efficiency~~ [%] and BOD_5/COD ratio behaviour after photocatalysis as OMW pre-treatment method, using TiO_2, Fe-TiO_2, Cr-TiO_2 and Fe-Cr-TiO_2 photocatalysts (3 h of solar light irradiation).

According to the above discussed results, the subsequent H_2O_2-assisted photocatalysis tests were carried out in presence of the oxidant dosage equal to 0.75 g L^{-1} using the doped photocatalysts Fe-TiO_2 and Fe-Cr-TiO_2, Fe^{3+} being present (as evidenced by XRD), which is a very well-known photo-Fenton like catalyst [68].

Fe-Cr-TiO_2 photocatalyst, in presence of H_2O_2, allowed to simultaneously achieve the highest removal efficiency of the three parameters: TPHs (66%), COD (29%) and BOD_5 (15%) (Figure 6). This behavior could be attributed to the lower band gap of Fe-Cr-TiO_2, induced by the presence of

Cr^{3+} inside the TiO_2 lattice, which results in a higher absorption feature of the visible fraction of the simulated sunlight. As a consequence the reduction of Fe^{3+} to Fe^{2+} by photoexcited electrons is promoted in a more effective way with respect to Fe-TiO_2, yielding Fe^{2+} that can react with H_2O_2 to generate hydroxyl radicals [68].

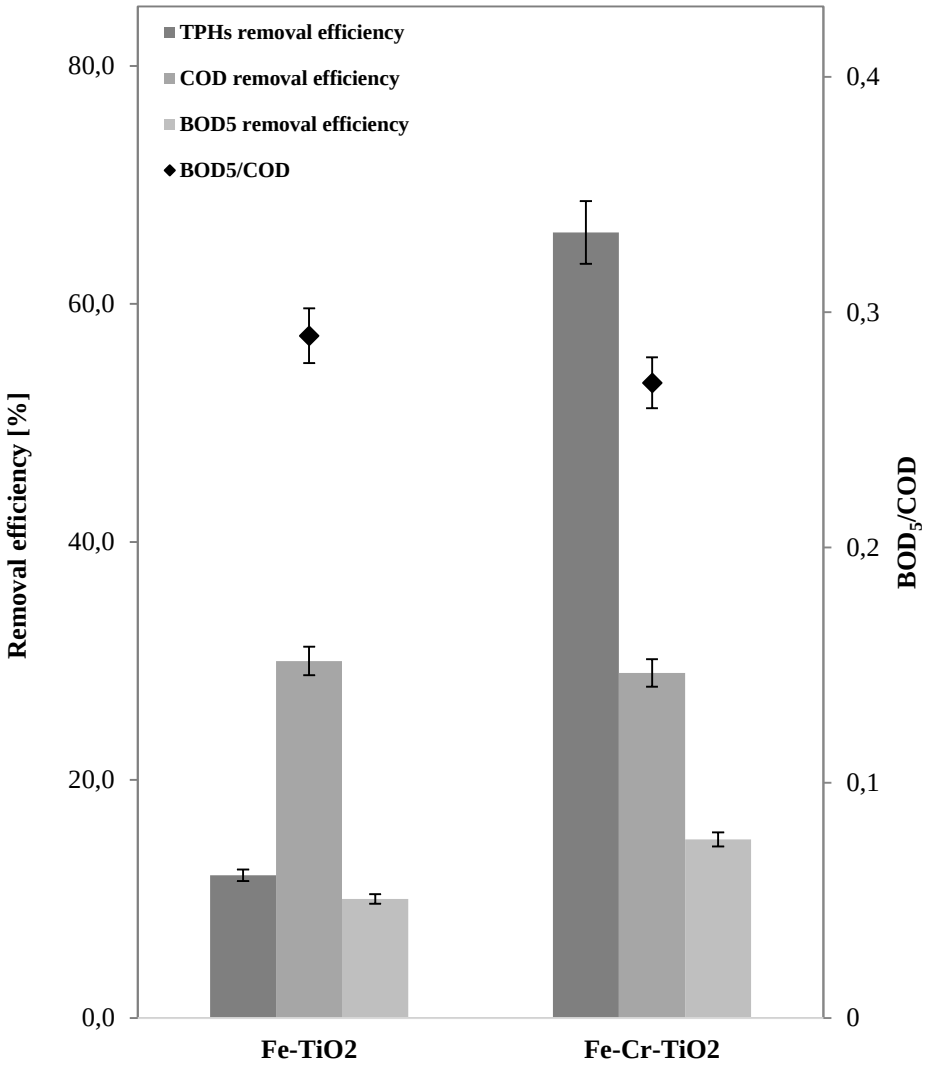

Figure 6. TPHs, COD, BOD_5 removal ~~efficiency~~ [%] and BOD_5/COD by photocatalysis as OMW pre-treatment method, using Fe-TiO_2 and Fe-Cr-TiO_2 photocatalysts with a dosage of H_2O_2 equal to 0.75 g L^{-1}, after 3 h of solar light irradiation.

Afterwards, experimental tests were carried out varying the H_2O_2 dosage with Fe-Cr-TiO_2 catalyst (Figure 7). As H_2O_2 dosage was decreased from 0.75 g L^{-1} to 0.50 g L^{-1}, an increase of TPHs removal

~~efficiency~~ as well as an improvement in the OMW biodegradability was observed (0.22 to 0.33) without leaching of either Fe or Cr in the treated solutions. A similar increase in biodegradability (0.16 to 0.26) was found in a study on the combined use of Coagulation and Fenton for the treatment of OMW [69]. Similarly, in another study coagulation and Fenton-like treatment led to an increase in biodegradability from 0.11 to 0.33 [70]. Moreover, the use of optimal operating conditions for the biodegradability increase and TPHs removal would allow to increase the performances of a subsequent biological process allowing the treatment of larger volume of OMW. According to a previous study, the combination of a heterogeneous photocatalytic process with MBBR resulted in an effective treatment of coal gasification wastewater (characterized by high TPHs concentration (80–120 mg/L) and low biodegradability (0.05–0.08 of BOD_5/COD)). In particular, in this study, not only the heterogeneous photocatalytic process significantly increased the biodegradability of wastewater (0.49 of BOD_5/COD) reducing the TPHs content (65%), but the subsequent treatment with MBBR showed higher and faster total organic carbon removal [71].

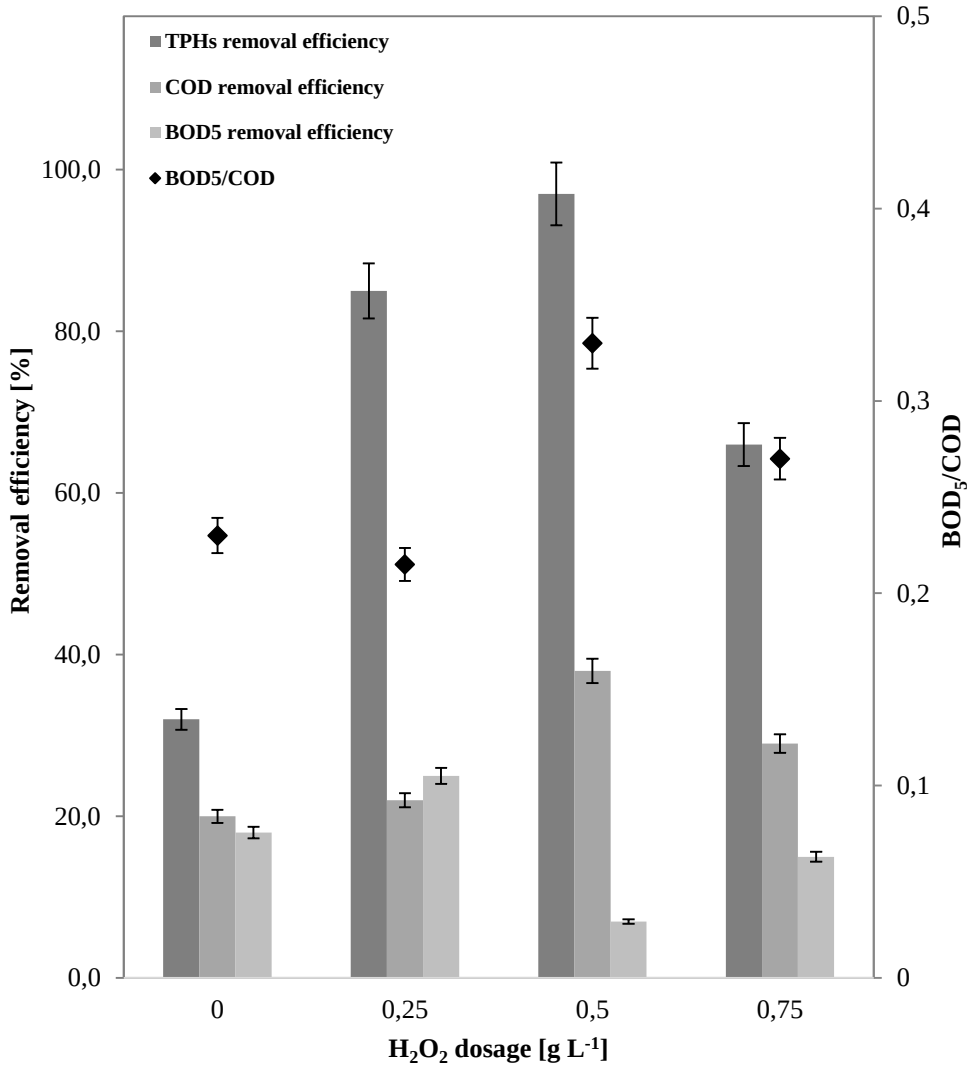

Figure 7. TPHs, COD and BOD_5 removal ~~efficiency~~ [%] and BOD_5/COD behaviour after photocatalysis application as OMW pre-treatment method using Fe-Cr-TiO_2 photocatalyst after 3h of solar light irradiation: effect of H_2O_2 dosage [g L^{-1}]

The further reduction of H_2O_2 dosage to 0.25 g L^{-1} resulted in a decreased photocatalytic activity, making 0.50 g L^{-1} the optimal oxidant dosage in terms of TPHs and COD removal ~~efficiency~~ (97% and 38%, respectively) and improved biodegradability of OMW. The influence of H_2O_2 dosage on the target parameters can be explained by the formation of hydroxyl radicals ($^{\bullet}OH$) and their conversion into hydroperoxide radicals ($HO_2^{\bullet}$) [72-74]. Hydrogen peroxide can interact with the photo-induced electrons in the conduction band, leading to an increase in the concentration of hydroxyl radicals [75] (reactions A and B):

$$H_2O_2 + e^- \rightarrow {}^{\bullet}OH + OH^- \quad (A)$$

$$H_2O_2 + O_2^{-\bullet} \rightarrow {}^{\bullet}OH + OH^- + O_2 \quad (B)$$

$$H_2O_2 + {}^{\bullet}OH \rightarrow H_2O + HO_2^{\bullet} \quad (C)$$

$$HO_2^{\bullet} + {}^{\bullet}OH \rightarrow H_2O + O_2 \quad (D)$$

Consequently, the addition of hydrogen peroxide in the photocatalytic system promotes the degradation of the organic compounds present in the solution. However, by exceeding the optimal dosage of H_2O_2, the excess of hydrogen peroxide favours the conversion of hydroxyl radicals into hydroperoxide radicals (reaction C), which are weaker oxidants than hydroxyl radicals [76], promoting also a termination reaction with hydroxyl radicals (reaction D) [77], which leads to a decrease in the concentration of reactive oxygen species in the aqueous solution.

3.2.3 OMW post-treatment by photocatalysis

Photocatalytic process using TiO_2, Fe-TiO_2, Cr-TiO_2, and Fe-Cr-TiO_2 was also investigated as possible polishing step after biological treatment by MBBR of OMW mixed to SWW (TOMW), in order to check the possibility to make the effluent in compliance with standard for disposal into surface water. As expected, the lower initial polluting loading of TOMW compared to OMW allowed to increase TPHs, COD, and BOD_5 removal efficiencies by photocatalytic tests (Figure 8).

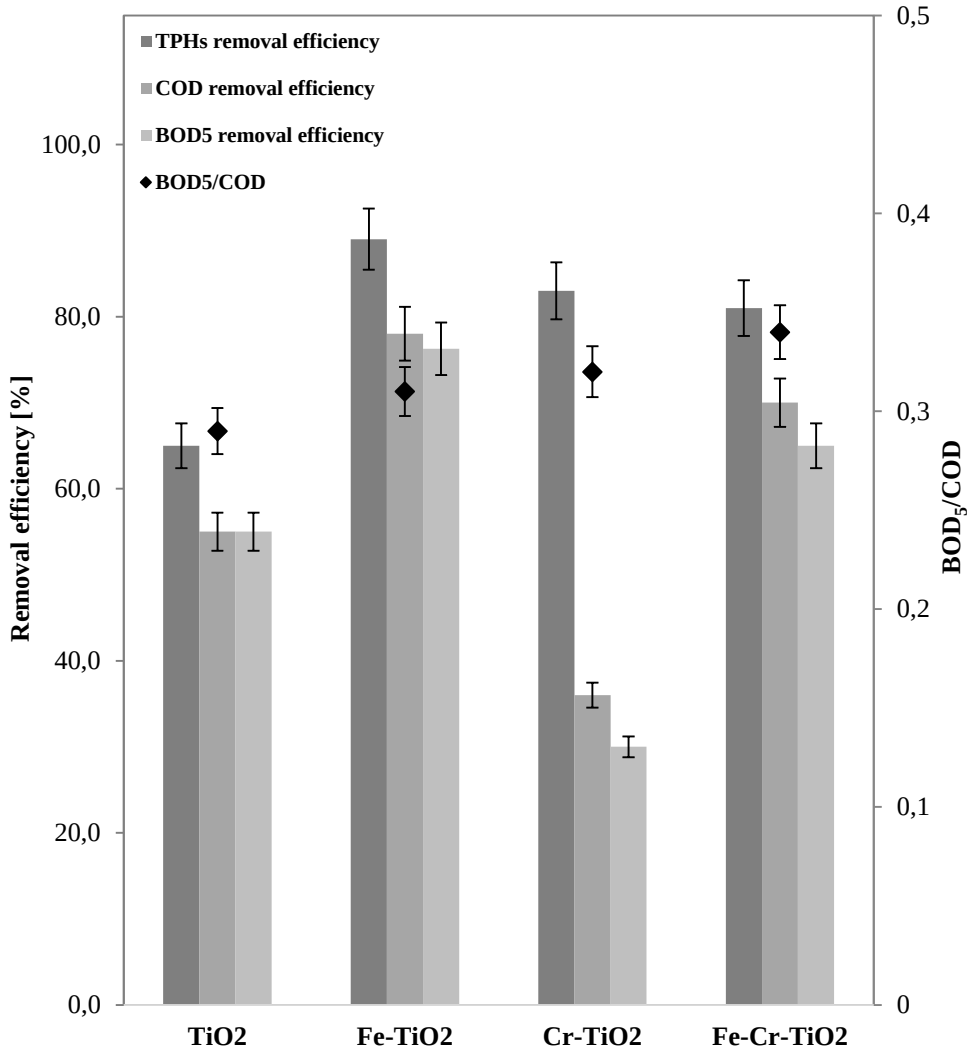

Figure 8. TPHs, COD, BOD_5 removal ~~efficiency~~ [%] and BOD_5/COD behaviour after photocatalysis as OMW post-treatment method (TOMW), using TiO_2, Fe-TiO_2, Cr-TiO_2 and Fe-Cr-TiO_2 photocatalysts after 3 h of solar light irradiation.

The obtained results can be explained considering that the biological process carried out upstream of the photocatalytic process, reduced the initial concentration of pollutants present in wastewater and therefore allowed to increase the photocatalytic activity of the photocatalyst. The presence of a higher concentration of pollutants inside the solution may led to a decrease in the active sites of the photocatalyst available for the pollutant molecules or to an increase in the screening phenomenon that limited the penetration of light radiation [78, 79]. In photocatalysis, among all the synthesized photocatalysts, Fe-TiO_2 showed the best activity in the degradation of compounds present in TOMW,

exhibiting a value of TPHs removal ~~efficiency~~ equal to 89% compared to the values of 83%, 81%, and 65% for Cr-TiO_2, Fe-Cr-TiO_2 and TiO_2 photocatalysts, respectively. Since the photoactivity showed in the presence of H_2O_2 by Fe-TiO_2 on OMW (Fig. 6) was higher with respect to COD removal, this catalyst was selected for the subsequent photocatalytic tests on TOMW, by varying the H_2O_2 dosage from 0.25 g L^{-1} up to 0.75 g L^{-1} (Figure 9).

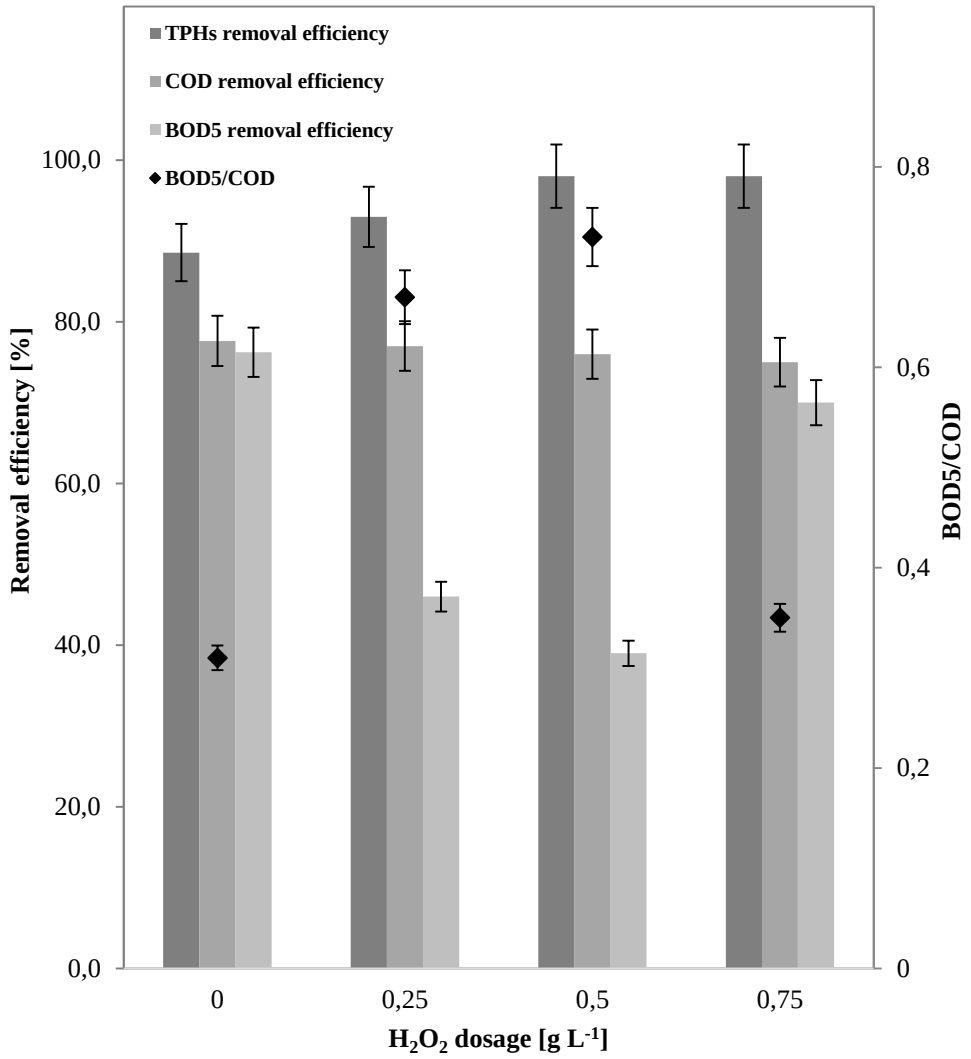

Figure 9. TPHs, COD and BOD_5 removal ~~efficiency~~ [%] and BOD_5/COD behaviour after Fe-TiO_2 photocatalysis as OMW post-treatment method (TOMW) (3h of solar light irradiation): effect of H_2O_2 dosage [g L^{-1}].

The addition of H_2O_2 did not significantly improve the photocatalytic activity of Fe-TiO_2. As the H_2O_2 dosage was increased, a negligible decrease in COD removal ~~efficiency~~ was observed, whereas

a slight increase in TPHs removal ~~efficiency~~ from 89% (in the absence of H_2O_2) to 98% (with 0.5-0.75 g L^{-1} of H_2O_2) was obtained. Also in this case, the results of leaching test showed the absence of Fe in the treated solutions. The experimental results on photocatalytic process with Fe-TiO_2 on TOMW underlined that a satisfactory pollutants abatement degree cannot be achieved without the addition of H_2O_2 (Figure 11). In particular, for the experiment with 0.75 g L^{-1} of H_2O_2, the residual TPHs, COD and BOD_5 concentrations were respectively 0.3 mg L^{-1}, 68 mg L^{-1} and 24 mg L^{-1}, which are in compliance with the limit set by Italian regulation for effluent discharge into surface water (annex 5, third part, D.Lgs n. 152 /2006).

4 Conclusions

OMW are hard to treat by conventional methods and a multi-barrier approach is necessary to make the effluent in compliance with regulations for disposal into the environment. In this work a solar driven heterogeneous photocatalytic process was coupled to an MBBR with the aim to evaluate the feasibility as pre- or post-treatment of real OMW. Accordingly, photocatalytic tests in presence of metal-doped TiO_2 powders active under solar light with or without H_2O_2 as oxidant were carried out. A good removal of THPs, COD and BOD_5 combined with an increase in the biodegradability of OMW was observed with Fe-TiO_2 and Fe-Cr-TiO_2. When the photocatalytic process was investigated as pre-treatment to biological process, Fe-Cr-TiO_2 resulted in the best photocatalytic performance with TPHs removal as high as 97% and increased biodegradability (COD/BOD_5=0.33) in presence of H_2O_2 (optimum dosage 0.5g L^{-1}). A process with such high performances would allow to biologically treat larger volumes of OMW thanks to the reduced concentration of TPHs in input and to the greater biodegradability. On the other hand, when photocatalytic process was investigated as post-treatment of OMW (TOMW), ~~higher performance was observed in terms of process efficiency compared to the pre-treatment option, due to the lower initial polluting loading of TOMW compared~~

~~to OMW. In particular,~~ Fe-TiO_2 showed the best activity in the degradation of the target parameters and the addition of 0.75 g L^{-1} of H_2O_2 was sufficient to make the effluent in compliance with Italian regulation for effluent disposal into surface water. In conclusion, the combination between photocatalysis and MBBR can be an effective and perspective solution for a sustainable OMW treatment. In particular, the use of photocatalysis as polishing step after MBBR treatment looks the more attractive option, because the pre-treatment configuration would ask for a too high dilution of the real OMW (larger treatment volume and higher energy costs related to effluent recirculation) to make photocatalytic process effective.

References

[1] D.P. Minh, P. Gallezot, S. Azabou, S. Sayadi, M. Besson, Catalytic wet air oxidation of olive oil mill effluents: 4. Treatment and detoxification of real effluents, Applied Catalysis B: Environmental 84(3-4) (2008) 749-757.

[2] O. Meftah, Z. Guergueb, M. Braham, S. Sayadi, A. Mekki, Long term effects of olive mill wastewaters application on soil properties and phenolic compounds migration under arid climate, Agricultural Water Management 212 (2019) 119-125.

[3] A. Benamar, F. Mahjoubi, N. Barka, F. Kzaiber, K. Boutoial, G.A. Ali, A. Oussama, Olive mill wastewater treatment using infiltration percolation in column followed by aerobic biological treatment, SN Applied Sciences 2(4) (2020) 1-12.

[4] L. Davies, A. Vilhena, J. Novais, S. Martins-Dias, Modelling of olive mill wastewater characteristics, WIT Transactions on Ecology and the Environment 65 (2003).

[5] A.I. Vavouraki, M.V. Zakoura, M.A. Dareioti, M. Kornaros, Biodegradation of Polyphenolic Compounds from Olive Mill Wastewaters (OMW) during Two-stage anaerobic Co-digestion of Agro-industrial mixtures, Waste and Biomass Valorization 11(11) (2020) 5783-5791.

[6] P. Paraskeva, E. Diamadopoulos, Technologies for olive mill wastewater (OMW) treatment: a review, Journal of Chemical Technology & Biotechnology: International Research in Process, Environmental & Clean Technology 81(9) (2006) 1475-1485.

[7] R. Borja, F. Raposo, B. Rincón, Treatment technologies of liquid and solid wastes from two-phase olive oil mills, Grasas y aceites 57(1) (2006) 32-46.

[8] S. Zheng, J. Sun, H. Han, Effect of dissolved oxygen changes on activated sludge fungal bulking during lab-scale treatment of acidic industrial wastewater, Environmental science & technology 45(20) (2011) 8928-8934.

[9] J.M. Ochando-Pulido, A. Martinez-Ferez, On the recent use of membrane technology for olive mill wastewater purification, Membranes 5(4) (2015) 513-531.

[10] S. Hosseini, S. Borghei, The treatment of phenolic wastewater using a moving bed bio-reactor, Process biochemistry 40(3-4) (2005) 1027-1031.

[11] H. Zhou, G. Wang, M. Wu, W. Xu, X. Zhang, L. Liu, Phenol removal performance and microbial community shift during pH shock in a moving bed biofilm reactor (MBBR), Journal of hazardous materials 351 (2018) 71-79.

[12] M. Zheng, H. Zhu, Y. Han, C. Xu, Z. Zhang, H. Han, Comparative investigation on carbon-based moving bed biofilm reactor (MBBR) for synchronous removal of phenols and ammonia in treating coal pyrolysis wastewater at pilot-scale, Bioresource technology 288 (2019) 121590.

[13] A.M. Silva, E. Nouli, N.P. Xekoukoulotakis, D. Mantzavinos, Effect of key operating parameters on phenols degradation during H2O2-assisted TiO2 photocatalytic treatment of simulated and actual olive mill wastewaters, Applied Catalysis B: Environmental 73(1-2) (2007) 11-22.

[14] H. Gulyas, Processes for the removal of recalcitrant organics from industrial wastewaters, Water Science and Technology 36(2-3) (1997) 9-16.

[15] F. Chkili, M. Person, C. Colbeau-Justin, M. Abderrabba, The olive mill waste water decontamination with photocatalysis based on TiO2: effect of operational parameters, Biosci Biotech Res Asia 14(3) (2017) 933-944.

[16] W. Gernjak, M. Maldonado, S. Malato, J. Caceres, T. Krutzler, A. Glaser, R. Bauer, Pilot-plant treatment of olive mill wastewater (OMW) by solar TiO2 photocatalysis and solar photo-Fenton, Solar Energy 77(5) (2004) 567-572.

[17] C.A. García, G. Hodaifa, Real olive oil mill wastewater treatment by photo-Fenton system using artificial ultraviolet light lamps, Journal of Cleaner Production 162 (2017) 743-753.

[18] C. Agabo-García, N. Calderón, G. Hodaifa, Heterogeneous Photo-Fenton Reaction for Olive Mill Wastewater Treatment—Case of Reusable Catalyst, Catalysts 11(5) (2021) 557.
[19] F. Cuomo, F. Venditti, G. Cinelli, A. Ceglie, F. Lopez, Olive mill wastewater (OMW) phenol compounds degradation by means of a visible light activated titanium dioxide-based photocatalyst, Zeitschrift für Physikalische Chemie 230(9) (2016) 1269-1280.
[20] C. Byrne, G. Subramanian, S.C. Pillai, Recent advances in photocatalysis for environmental applications, Journal of Environmental Chemical Engineering 6(3) (2018) 3531-3555.
[21] M.R. Hoffmann, S.T. Martin, W. Choi, D.W. Bahnemann, Environmental applications of semiconductor photocatalysis, Chemical reviews 95(1) (1995) 69-96.
[22] I.K. Konstantinou, T.A. Albanis, TiO2-assisted photocatalytic degradation of azo dyes in aqueous solution: kinetic and mechanistic investigations: a review, Applied Catalysis B: Environmental 49(1) (2004) 1-14.
[23] K. Kowalska, G. Maniakova, M. Carotenuto, O. Sacco, V. Vaiano, G. Lofrano, L. Rizzo, Removal of carbamazepine, diclofenac and trimethoprim by solar driven advanced oxidation processes in a compound triangular collector based reactor: A comparison between homogeneous and heterogeneous processes, Chemosphere 238 (2020). https://doi.org/10.1016/j.chemosphere.2019.124665.
[24] V. Vaiano, O. Sacco, G. Libralato, G. Lofrano, A. Siciliano, F. Carraturo, M. Guida, M. Carotenuto, Degradation of anionic azo dyes in aqueous solution using a continuous flow photocatalytic packed-bed reactor: Influence of water matrix and toxicity evaluation, Journal of Environmental Chemical Engineering 8(6) (2020). https://doi.org/10.1016/j.jece.2020.104549.
[25] V. Vaiano, O. Sacco, D. Sannino, Electric energy saving in photocatalytic removal of crystal violet dye through the simultaneous use of long-persistent blue phosphors, nitrogen-doped TiO2 and UV-light emitting diodes, Journal of Cleaner Production 210 (2019) 1015-1021. https://doi.org/10.1016/j.jclepro.2018.11.017.
[26] A. Fujishima, T.N. Rao, D.A. Tryk, Titanium dioxide photocatalysis, Journal of photochemistry and photobiology C: Photochemistry reviews 1(1) (2000) 1-21.
[27] J. Schneider, M. Matsuoka, M. Takeuchi, J. Zhang, Y. Horiuchi, M. Anpo, D.W. Bahnemann, Understanding TiO2 photocatalysis: mechanisms and materials, Chemical reviews 114(19) (2014) 9919-9986.
[28] A. Fujishima, X. Zhang, D.A. Tryk, TiO2 photocatalysis and related surface phenomena, Surface science reports 63(12) (2008) 515-582.
[29] W. Choi, A. Termin, M.R. Hoffmann, The role of metal ion dopants in quantum-sized TiO2: correlation between photoreactivity and charge carrier recombination dynamics, The Journal of Physical Chemistry 98(51) (2002) 13669-13679.
[30] W. Li, Influence of electronic structures of doped TiO2 on their photocatalysis, physica status solidi (RRL)–Rapid Research Letters 9(1) (2015) 10-27.
[31] A. Mancuso, W. Navarra, O. Sacco, S. Pragliola, V. Vaiano, V. Venditto, Photocatalytic degradation of thiacloprid using tri-doped tio2 photocatalysts: A preliminary comparative study, Catalysts 11(8) (2021). https://doi.org/10.3390/catal11080927.
[32] A. Mancuso, O. Sacco, V. Vaiano, B. Bonelli, S. Esposito, F.S. Freyria, N. Blangetti, D. Sannino, Visible light-driven photocatalytic activity and kinetics of fe-doped tio2 prepared by a three-block copolymer templating approach, Materials 14(11) (2021). https://doi.org/10.3390/ma14113105.
[33] I. Ruzmanova, M. Ustundas, M. Stoller, A. Chianese, Photocatalytic treatment of olive mill wastewater by n-doped titanium dioxide nanoparticles under visible light, Chemical Engineering Transactions 32 (2013) 2233-2238.
[34] I. Seynure, F. Aliyev, M. Stoller, A. Chianese, Optimal Configuration of a Photocatalytic lab-reactor by using Immobilized Nanostructured TiO 2, Chemical Engineering Transactions 47 (2016) 199-204.
[35] A. Speltini, F. Maraschi, M. Sturini, V. Caratto, M. Ferretti, A. Profumo, Sorbents Coupled to Solar Light TiO2-Based Photocatalysts for Olive Mill Wastewater Treatment, International Journal of Photoenergy 2016 (2016).
[36] D.T. Sponza, R. Oztekin, Photodegradation of polyphenols and aromatic amines in olive mill effluents with Ni doped C/TiO2, Journal of Chemistry 2015 (2015).
[37] D.T. Sponza, R. Oztekin, Treatment of olive mill wastewater by photooxidation with ZrO2-doped TiO2 nanocomposite and its reuse capability, Environmental Technology 37(7) (2016) 865-879.
[38] A. Mancuso, O. Sacco, V. Vaiano, D. Sannino, S. Pragliola, V. Venditto, N. Morante, Visible light active Fe-Pr co-doped TiO2 for water pollutants degradation, Catalysis Today 380 (2021) 93-104.
[39] A.H. Hasan, F.H. Ali, Synthesis of Cr Doped TiO2 Using Sol-Gel Technique and Calculation of its Photocatalytic Activity, Indian Journal of Natural Sciences 9(51) (2018) 15242-15249.
[40] M. Freeda, G. Suresh, Structural and Luminescent properties of Eu-doped CaAl2O4 Nanophosphor by sol-gel method, Materials Today: Proceedings 4(2) (2017) 4260-4265.
[41] M. de Carluccio, A. Fiorentino, L. Rizzo, Multi-barrier treatment of mature landfill leachate: effect of Fenton oxidation and air stripping on activated sludge process and cost analysis, Journal of Environmental Chemical Engineering 8(5) (2020) 104444.
[42] M. Piculell, C. Suarez, C. Li, M. Christensson, F. Persson, M. Wagner, M. Hermansson, K. Jönsson, T. Welander, The inhibitory effects of reject water on nitrifying populations grown at different biofilm thickness, Water Research 104 (2016) 292-302.
[43] D. Sannino, V. Vaiano, O. Sacco, P. Ciambelli, Mathematical modelling of photocatalytic degradation of methylene blue under visible light irradiation, Journal of Environmental Chemical Engineering 1(1-2) (2013) 56-60.
[44] T. Wu, J.D. Englehardt, A new method for removal of hydrogen peroxide interference in the analysis of chemical oxygen demand, Environmental science & technology 46(4) (2012) 2291-2298.
[45] J. Box, Investigation of the Folin-Ciocalteau phenol reagent for the determination of polyphenolic substances in natural waters, Water research 17(5) (1983) 511-525.
[46] E. Jeong, P.H. Borse, J. Jang, J. Lee, O.-S. Jung, H. Chang, J. Jin, M. Won, H. Kim, Hydrothermal synthesis of Cr and Fe co-doped TiO2 nanoparticle photocatalyst, Journal of Ceramic Processing Research 9(3) (2008) 250-253.

[47] H.M. Yadav, T.V. Kolekar, S.H. Pawar, J.-S. Kim, Enhanced photocatalytic inactivation of bacteria on Fe-containing TiO2 nanoparticles under fluorescent light, Journal of Materials Science: Materials in Medicine 27(3) (2016) 1-9.
[48] J. Choi, H. Park, M.R. Hoffmann, Effects of single metal-ion doping on the visible-light photoreactivity of TiO2, The Journal of Physical Chemistry C 114(2) (2010) 783-792.
[49] H. Yadav, T. Kolekar, A. Barge, N. Thorat, S. Delekar, B. Kim, B. Kim, J. Kim, Enhanced visible light photocatalytic activity of Cr3+-doped anatase TiO2 nanoparticles synthesized by sol–gel method, Journal of Materials Science: Materials in Electronics 27(1) (2016) 526-534.
[50] C.-C. Tsai, H. Teng, Chromium-doped titanium dioxide thin-film photoanodes in visible-light-induced water cleavage, Applied Surface Science 254(15) (2008) 4912-4918.
[51] X. Li, Z. Guo, T. He, The doping mechanism of Cr into TiO 2 and its influence on the photocatalytic performance, Physical Chemistry Chemical Physics 15(46) (2013) 20037-20045.
[52] G. Colón, M. Maicu, M.s. Hidalgo, J. Navío, Cu-doped TiO2 systems with improved photocatalytic activity, Applied Catalysis B: Environmental 67(1-2) (2006) 41-51.
[53] H. Liu, L. Gao, Preparation and properties of nanocrystalline α-Fe2O3-sensitized TiO2 nanosheets as a visible light photocatalyst, Journal of the American Ceramic Society 89(1) (2006) 370-373.
[54] A. Chanda, K. Rout, M. Vasundhara, S.R. Joshi, J. Singh, Structural and magnetic study of undoped and cobalt doped TiO 2 nanoparticles, RSC advances 8(20) (2018) 10939-10947.
[55] J.H. Lee, Y.S. Yang, Synthesis of TiO 2 nanoparticles with pure brookite at low temperature by hydrolysis of TiCl 4 using HNO 3 solution, Journal of materials science 41(2) (2006) 557-559.
[56] W. Li, L. Xie, L. Zhou, J. Ochoa-Lozano, C. Li, X. Chai, A systemic study on Gd, Fe and N co-doped TiO2 nanomaterials for enhanced photocatalytic activity under visible light irradiation, Ceramics International 46(15) (2020) 24744-24752.
[57] K.A. Michalow, E.H. Otal, D. Burnat, G. Fortunato, H. Emerich, D. Ferri, A. Heel, T. Graule, Flame-made visible light active TiO2: Cr photocatalysts: correlation between structural, optical and photocatalytic properties, Catalysis today 209 (2013) 47-53.
[58] L. Li, Z.F. Yan, G.Q. Lu, Z.H. Zhu, Synthesis and structure characterization of chromium oxide prepared by solid thermal decomposition reaction, The Journal of Physical Chemistry B 110(1) (2006) 178-183.
[59] R. Dubey, S. Singh, Investigation of structural and optical properties of pure and chromium doped TiO2 nanoparticles prepared by solvothermal method, Results in physics 7 (2017) 1283-1288.
[60] I. Ganesh, P.P. Kumar, A.K. Gupta, P.S. Sekhar, K. Radha, G. Padmanabham, G. Sundararajan, Preparation and characterization of Fe-doped TiO 2 powders for solar light response and photocatalytic applications, Processing and application of ceramics 6(1) (2012) 21-36.
[61] A. Mancuso, O. Sacco, D. Sannino, S. Pragliola, V. Vaiano, Enhanced visible-light-driven photodegradation of Acid Orange 7 azo dye in aqueous solution using Fe-N co-doped TiO2, Arabian Journal of Chemistry 13(11) (2020) 8347-8360.
[62] M. Mohammadtaheri, Q. Yang, Y. Li, J. Corona-Gomez, The effect of deposition parameters on the structure and mechanical properties of chromium oxide coatings deposited by reactive magnetron sputtering, Coatings 8(3) (2018) 111.
[63] P. Panta, C. Bergmann, Raman spectroscopy of iron oxide of nanoparticles (Fe3O4), J. Mater. Sci. Eng 5(3) (2015).
[64] R.A. Solano, A.P. Herrera, D. Maestre, A. Cremades, Fe-TiO2 nanoparticles synthesized by green chemistry for potential application in waste water photocatalytic treatment, Journal of Nanotechnology 2019 (2019).
[65] S.P. Takle, O.A. Apine, J.D. Ambekar, S.L. Landge, N.N. Bhujbal, B.B. Kale, R.S. Sonawane, Solar-light-active mesoporous Cr–TiO 2 for photodegradation of spent wash: an in-depth study using QTOF LC-MS, RSC advances 9(8) (2019) 4226-4238.
[66] Y.-Q. Gu, T.-T. Li, H.-Q. Li, Biofilm formation monitored by confocal laser scanning microscopy during startup of MBBR operated under different intermittent aeration modes, Process biochemistry 74 (2018) 132-140.
[67] S.N.H.A. Bakar, H.A. Hasan, A.W. Mohammad, S.R.S. Abdullah, R. Ngteni, K.M.M. Yusof, Performance of a laboratory-scale moving bed biofilm reactor (MBBR) and its microbial diversity in palm oil mill effluent (POME) treatment, Process Safety and Environmental Protection 142 (2020) 325-335.
[68] A. Abdelhaleem, W. Chu, Prediction of carbofuran degradation based on the hydroxyl radical's generation using the FeIII impregnated N doped-TiO2/H2O2/visible LED photo-Fenton-like process, Chemical Engineering Journal 382 (2020) 122930.
[69] A. Alver, E. Baştürk, A. Kılıç, M. Karataş, Use of advance oxidation process to improve the biodegradability of olive oil mill effluents, Process Safety and Environmental Protection 98 (2015) 319-324.
[70] B.M. Esteves, C.S. Rodrigues, F. Maldonado-Hódar, L.M. Madeira, Treatment of high-strength olive mill wastewater by combined Fenton-like oxidation and coagulation/flocculation, Journal of Environmental Chemical Engineering 7(4) (2019) 103252.
[71] P. Xu, H. Han, B. Hou, H. Zhuang, S. Jia, D. Wang, K. Li, Q. Zhao, The feasibility of using combined TiO2 photocatalysis oxidation and MBBR process for advanced treatment of biologically pretreated coal gasification wastewater, Bioresource Technology 189 (2015) 417-420.
[72] V.K. Gupta, R. Jain, S. Agarwal, M. Shrivastava, Kinetics of photo-catalytic degradation of hazardous dye Tropaeoline 000 using UV/TiO2 in a UV reactor, Colloids and Surfaces A: Physicochemical and Engineering Aspects 378(1-3) (2011) 22-26.
[73] E.R. Bandala, S. Gelover, M.T. Leal, C. Arancibia-Bulnes, A. Jimenez, C.A. Estrada, Solar photocatalytic degradation of Aldrin, Catalysis Today 76(2-4) (2002) 189-199.
[74] E. Bizani, K. Fytianos, I. Poulios, V. Tsiridis, Photocatalytic decolorization and degradation of dye solutions and wastewaters in the presence of titanium dioxide, Journal of Hazardous Materials 136(1) (2006) 85-94.
[75] D.-H. Tseng, L.-C. Juang, H.-H. Huang, Effect of oxygen and hydrogen peroxide on the photocatalytic degradation of monochlorobenzene in aqueous suspension, International Journal of Photoenergy 2012 (2012).
[76] M.P. Rayaroth, U.K. Aravind, C.T. Aravindakumar, Degradation of pharmaceuticals by ultrasound-based advanced oxidation process, Environmental Chemistry Letters 14(3) (2016) 259-290.

650 [77] D.D. Dionysiou, M.T. Suidan, E. Bekou, I. Baudin, J.-M. Laîné, Effect of ionic strength and hydrogen peroxide on the photocatalytic
651 degradation of 4-chlorobenzoic acid in water, Applied Catalysis B: Environmental 26(3) (2000) 153-171.
652 [78] L. Andronic, A. Enesca, C. Vladuta, A. Duta, Photocatalytic activity of cadmium doped TiO2 films for photocatalytic degradation
653 of dyes, Chemical Engineering Journal 152(1) (2009) 64-71.
654 [79] N. Venkatachalam, M. Palanichamy, B. Arabindoo, V. Murugesan, Enhanced photocatalytic degradation of 4-chlorophenol by
655 Zr4+ doped nano TiO2, Journal of Molecular Catalysis A: Chemical 266(1-2) (2007) 158-165.
656
657